THE JOURNAL OF PHYSICAL CHEMISTRY C

Article

Cite This: J. Phys. Chem. C 2019, 123, 22250−22260

pubs.acs.org/JPCC

Comparative Study of the Different Anchoring of Organometallic Dyes on Ultrathin Alumina

Wolf-Dietrich Zabka,[†] Tiziana Musso,[‡] Mathias Mosberger,[‡] Zbynek Novotny,[†,§] Roberta Totani,[†] Marcella Iannuzzi,[‡] Benjamin Probst,[‡] Roger Alberto,[‡] and Jürg Osterwalder*[,†]

[†]Physik-Institut, and [‡]Institut für Chemie, Universität Zürich, Winterthurerstrasse 190, 8057 Zürich, Switzerland

[§]Paul Scherrer Institut, 5232 Villigen, Switzerland

Supporting Information

ABSTRACT: Significant improvements in incident photon-to-current efficiencies can be obtained by covering inorganic semiconductors with ultrathin alumina films and sensitizing them with adsorbed dye molecules. The anchoring mode of the latter to the substrate affects the charge transport between the dye and the electrode via tunneling, and consequently, the device efficiency. In this work, we employ X-ray and ultraviolet photoelectron spectroscopies (XPS and UPS) for a comparative study of the adsorption of three rhenium and two ruthenium organometallic dyes, one of each being ionic, with different anchoring modes on single-crystalline ultrathin alumina films. Molecular monolayers were prepared by self-assembly from solution. Quantitative XPS analysis reveals higher surface densities for the Re dyes. Nearly stoichiometric coadsorption of counterions is observed for the ionic dyes. Density functional theory (DFT) calculations for the Re dyes show that the most stable adsorption configurations exhibit the expected bonding via the dedicated anchoring groups (carboxyls or methylphosphonic acid), with an additional sulfur−aluminum bond for the dyes containing a thiocyanate ligand. The alignment of the occupied molecular levels with respect to the alumina valence band maximum, obtained for these geometries, follows the experimental trend in the UPS data and places the lowest unoccupied molecular orbitals (LUMOs) close to the Fermi level of the systems, far inside the alumina band gap. Dynamical charge screening is found to be important for this type of system when comparing UPS and DFT results. This work provides a general guideline for the systematic characterization of related molecules on surfaces.

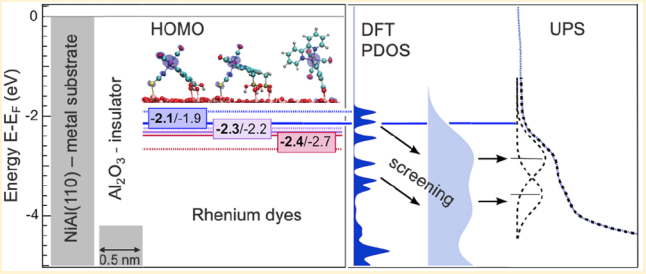

INTRODUCTION

Molecular systems have great potential for applications in dye-sensitized solar cells[1,2] for electric power generation and in dye-sensitized photoelectrochemical (PEC) cells[3−5] for energy conversion and storage. The robust anchoring of the dye molecules is crucial to ensure their stable coupling to the substrate and to enable the transport of charges between molecules and substrate,[6] most importantly in the harsh chemical environment of a PEC cell. Most previous experimental studies that aimed at the understanding of the anchoring mode at the molecular scale, typically based on surface science methods like photoelectron and X-ray spectroscopies and scanning tunneling microscopy, focused exclusively on the dye/titania interface.[7−13] Recently, several studies emphasized the role of ultrathin insulating alumina layers, which can reduce charge carrier recombination[14−19] and thus apparently promote charge carrier separation. It is argued that charge transfer to the underlying semiconductor occurs via tunneling through the alumina barrier, which requires a well-defined coupling of the dye to the alumina surface. Computational efforts on the dye/alumina/titania system indicated that the adsorption geometry of the dyes is altered by interfacial alumina layers, as was shown for the ruthenium-based N3 dye [*cis*-diisothiocyanato-bis(2,2′-bipyridyl-4,4′-dicarboxylic acid) ruthenium(II)].[20−22] Most studies focused only on one exemplary molecule, rather than comparing the properties of a group of molecules with systematic modifications. In order to further substantiate the tunneling picture, the alignment of the frontier orbitals with respect to the alumina band edges needs to be established, as well as their spatial distribution within the adsorbed molecules. It is the scope of this paper to provide such information for a selected group of dyes with different anchoring modes on alumina surfaces.

For this purpose, we studied the adsorption of five organometallic dyes on a crystalline and atomically flat alumina film with X-ray photoelectron spectroscopy (XPS), ultraviolet photoelectron spectroscopy (UPS), and density functional theory (DFT) calculations. The alumina film is ultrathin and has two atomic aluminum−oxygen bilayers (hence termed 2L-alumina in this work). It is grown by selective oxidation of a NiAl(110) single crystal. Its structure was described previously

Received: May 31, 2019
Revised: July 22, 2019
Published: August 20, 2019

DOI: 10.1021/acs.jpcc.9b05209
J. Phys. Chem. C 2019, 123, 22250−22260

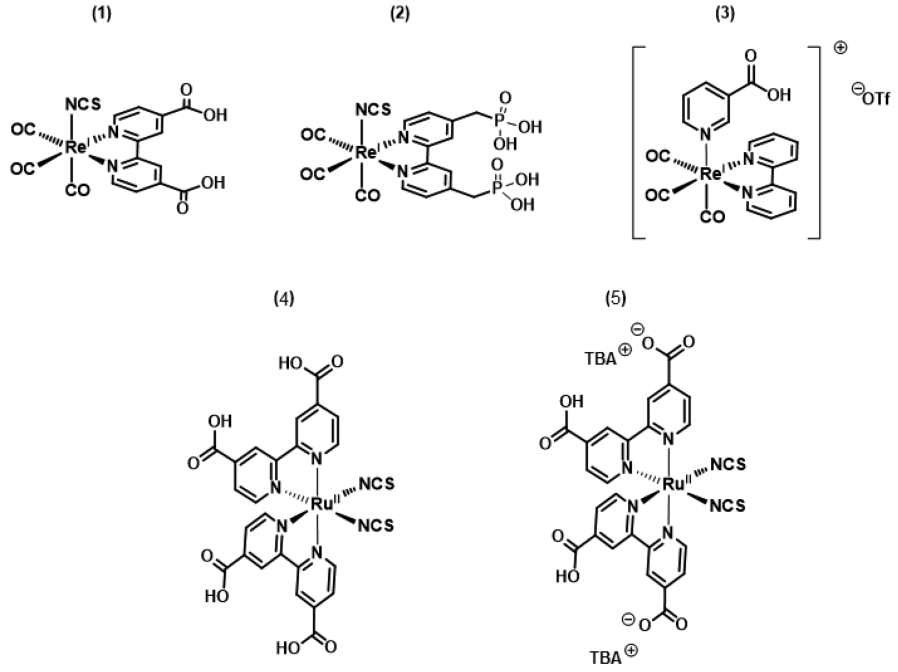

Figure 1. Structures of the used organometallic dyes.

in detail by Jaeger et al.[23] and Kresse et al.[24] In real devices, conformal ultrathin alumina films are typically grown by atomic layer deposition (ALD), which produces amorphous material. While the 2L-alumina on NiAl(110) is clearly crystalline with a high degree of long-range order,[25] the unit cell is large, exposing numerous different Al−O configurations as bonding sites for molecule adsorption. It can thus be considered a viable proxy for ALD-grown alumina, and yet it can be treated by DFT codes.

We compare the adsorption configurations, the packing densities, and the molecular energy levels of three systematically modified rhenium-based dye molecules, as well as two prototypical ruthenium dyes. Figure 1 shows the chemical structures of the considered dye molecules. The dye **1** is $[Re(NCS)(CO)_3(DCO_2bipy)]$ (DCO_2bipy = 2,2′-bipyridine-4,4′-dicarboxylic acid), which was previously used by our group to demonstrate the functionalization of 2L-alumina by self-assembly from solution.[26] Molecule **2** is $[Re(NCS)(CO)_3(DMPO_3bipy)]$ [$DMPO_3bipy$ = 2,2′-bipyridine-4,4′-bis(methylphosphonic acid)], where the carboxyl linkers are replaced by methylphosphonic acid linkers. Molecule **3** is $[Re(niacin)(CO)_3(bipy)]$ (bipy = 2,2′-bipyridine), where anionic thiocyanate (NCS) is replaced by a neutral niacin group, allowing for surface binding. The positive charge on dye **3** is compensated by a trifluoromethanesulfonate (OTf) anion. Molecule **4** is the prototypical N3 dye, which has a ruthenium center. The organometallic dye **5** is N719, a deprotonated version of N3 with two tetrabutylammonium (TBA) counterions.

In the case of dye **1**, the highest occupied molecular orbital (HOMO) and lowest unoccupied molecular orbital (LUMO) are localized deep inside the band gap of alumina,[26] and charge injection from the LUMO through the 2L-alumina into the metallic NiAl(110) is in principle possible via tunneling. Kinetically, this should be facilitated as in the case of dye **4**, which features the exact same binding ligand as dye **1** and where the LUMO is known to be localized on the DCO_2bipy ligand[18,27] and to extend into the semiconductor support in the case of TiO_2.[2]

Dye **2** is equipped with two phosphonic acid anchors for surface binding, allowing for a stronger interaction with the surface.[2] It has similar frontier orbitals, but is expected to show slower kinetics for electron injection due to the less conductive character of the methylphosphonic acid groups.[6,28] As for dye **3**, binding would be expected to occur through one carboxylic acid group in the axial niacin moiety, thus placing the HOMO much closer to the surface than the bipy localized LUMO.[29−31] In principle, this could allow for the reverse hole injection reaction into the excited dye.

As opposed to the neutral dyes **1**, **2**, and **4**, dye **3** is cationic due to the neutral ligands and the positive charge on the rhenium, while dye **5** is anionic, due to two deprotonated DCO_2bipy groups. This is compensated by a negatively charged trifluoromethansulfonate (OTf) for dye **3**, and by two positively charged tetrabutylammonium (TBA) ions for dye **5**. It will be of interest to see how point charges influence the energy level alignment of those dyes relative to each other.

In this work we will quantify the electronic level alignment between the different dyes and the 2L-alumina/NiAl(110) as a function of (i) the conductivity of the anchoring bipy ligand (dye **1** vs dye **2**), (ii) the orientation of the anchoring ligand (dye **1** vs dye **3**), and (iii) the presence or not of point charges (dye **3** vs dye **1** and dye **5** vs dye **4**). This will be done by a combined experimental and theoretical study using UPS data and DFT calculations. Great care has been taken in the preparation of clean molecular adlayers, using self-assembly from solutions and subsequent rinsing with solvent in a dedicated chamber attached to the photoemission spectrometer, followed by a detailed XPS characterization of the monolayers and their densities, as well as the absorption of counterions in the cases of dyes **3** and **5**.

DOI: 10.1021/acs.jpcc.9b05209
J. Phys. Chem. C 2019, 123, 22250−22260

METHODS

Sample Preparation. Experiments were conducted in a user-modified Vacuum Generators ESCALAB photoelectron spectrometer and ultrahigh-vacuum (UHV) system.[32] The ultrathin 2L-alumina films were grown on single-crystalline NiAl(110) substrates, as described by Zabka et al.[25] The molecules were deposited from solution in a dedicated vacuum chamber[26] in order to avoid exposure of the surfaces to air. To this end, the freshly grown and clean alumina films were transferred inside the vacuum system into this chamber, which was then brought into pressure equilibrium with the vapor pressure of the solvent. The 2L-alumina/NiAl(110) samples were rinsed three times with 0.1 mM solution of the rhenium molecules dissolved in acetonitrile (CH_3CN) to form multilayers. After that, the samples were rinsed three times with pure CH_3CN to remove physisorbed molecules, and a monolayer of chemisorbed molecules was left on the surface, as described previously by our group.[26] After pump down of the chamber, the samples could be transferred under vacuum back into the UHV system for surface characterization. For the ruthenium dyes, the solution was oversaturated due to the limited solubility of the molecules in CH_3CN. Details about the synthesis of the rhenium dyes can be found in the Supporting Information (section S10). The ruthenium dyes were obtained from Solaronix SA.

Photoelectron Spectroscopy. All photoemission experiments were performed at normal emission. UPS was conducted with a monochromatized He Iα source (photon energy of 21.22 eV). For XPS, a non-monochromatized Mg Kα source was used, providing photons with an energy of $h\nu$ = 1253.6 eV. The energy scale of the spectra was calibrated as described by Seah.[33] The thickness of the alumina films was determined based on the Al^{3+} shoulder of the Al 2p peak as described in our earlier work.[25]

In this paper, the areal density describes the number of particles (atoms or molecules) per area. We determine the areal density of rhenium atoms $N_{(Re)}$ for molecule **3** by comparing the intensity of the Re 4f peak (I_{Re}) to the intensities of several peaks (3s−4p) from a polycrystalline silver reference sample (I_{Ag}) according to

$$N_{Re} = \frac{I_{Re}}{\sigma_{Re}}\frac{\sigma_{Ag}}{I_{Ag}}\lambda_{Ag}\cos(\theta)n_{Ag} = \frac{I_{Re}}{\sigma_{Re}}A \quad (1)$$

θ is the emission angle of the photoelectrons with respect to the surface normal, σ_X is the corresponding photoionization cross section,[34] and n_{Ag} is the density of silver atoms (58.7/nm^3). The inelastic mean free path λ_{Ag} is calculated from the predictive Tanuma−Powell−Penn equation.[35]

The areal density of other atomic species was calculated by comparing the intensities of the respective peaks to the intensity of the Re 4f peak of molecule **3**. The intensities were normalized to the Ni 3p and Al 2p substrate peaks. The different photoionization cross sections[34] were considered for the respective peaks. The areal density of the molecules $\bar{N}$ was calculated with the weighted mean of n atomic densities x_i with errors of σ_i (based on the N 1s, S 2p, Re 4f, and Ru $3d_{5/2}$ peaks):

$$\bar{N} = \frac{\sum_{i=1}^{n}(x_i\sigma_i^{-2})}{\sum_{i=1}^{n}\sigma_i^{-2}} \quad (2)$$

The error $\sigma_{\bar{N}}$ of $\bar{N}$ was calculated by

$$\sigma_{\bar{N}} = \sqrt{\frac{1}{\sum_{i=1}^{n}\sigma_i^{-2}}} \quad (3)$$

The molecule diameter d on the surface was calculated by

$$d = \sqrt{\frac{2}{\sqrt{3N}}} \quad (4)$$

assuming close packing of the molecules.

The thicknesses of dye multilayers, as described by the number n_{ML} of molecular monolayers, were estimated by using the approximate equation

$$n_{ML} = \frac{(I_{Re4f}^{multilayer})(I_{substrate}^{monolayer})}{(I_{Re4f}^{monolayer})(I_{substrate}^{multilayer})} \quad (5)$$

where $I_{substrate}^{monolayer}$ refers to the sum of $I_{Al2p}^{monolayer} + I_{Ni3p}^{monolayer}$ and the same holds accordingly for the intensities for the multilayer.

Computational Methods. The CP2K suite of programs has been used for all simulations.[36] The Perdew−Burke−Ernzerhof (PBE) exchange correlation functional[37] has been used in conjunction with the Goedecker-type pseudopotentials[38] with 3, 18, 4, 5, 6, 15, and 6 valence electrons for Al, Ni, C, N, S, Re, and O, respectively, where the Kohn−Sham orbitals are expanded in a double-ζ-valence plus polarization (DZVP) Gaussian-type basis set.[39] The Poisson equation has been solved in reciprocal space within the Gaussian and plane waves framework (GPW).[40] The Grimme's D3 correction[41] has been used to account for the dispersion interactions. The hybrid functionals PBE0[42,43] and HSE06[44] have been used to get more accurate density of states.

For the structural optimization and the calculation of adsorption energies, our model starts with a clean, non-hydroxylated surface. Several possible initial conditions were considered for the structural optimization of the adsorbed molecules. By choosing the initial state, we positioned the molecule relatively close to the surface, assuming an initial orientation, and favoring certain interactions (e.g., metal−oxygen) by proximity. Our structure search was thus guided by chemical intuition and cannot be considered complete, since we did not explore the whole configurational space.

Solvent effects were not considered. The solvent might play a role during the deposition process, but the investigation of the specific reaction process is beyond the scope of this work. Our final structures are compared to experiments performed in UHV, with XPS showing no traces of CH_3CN residuals left on the surface. In order to take into account H dissociation, we removed the hydrogen atoms completely. Only in the case of dye **1**, we also provide an approximate estimate of the activation energy for the dissociation of H from COOH (see Supporting Information, section S5). For comparison of the adsorption energies of nondissociative and dissociative adsorption, the reference state for the removed atoms, i.e., the hydrogens, is taken as the H_2 molecule in the gas phase. The dissociative adsorption for individual carboxyl linkers thus refers to a reaction of the type

$$\cdots\text{−M−O−M−}\cdots + \text{R−CO−OH} \rightarrow \cdots\text{−M−O−M−O−CO−R} + \frac{1}{2}H_2$$

DOI: 10.1021/acs.jpcc.9b05209
J. Phys. Chem. C 2019, 123, 22250−22260

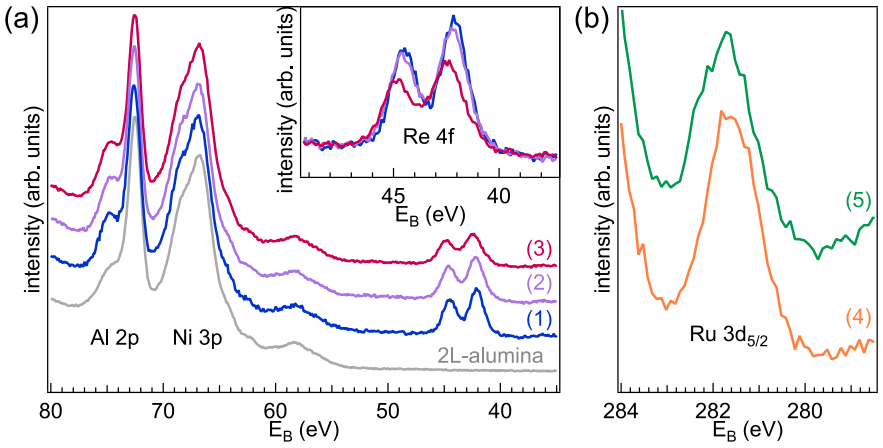

Figure 2. (a) XPS data (Mg Kα) of Al 2p, Ni 3p, and Re 4f peaks for 2L-alumina (gray) and monolayers of molecule **1** (blue), **2** (violet), and **3** (red). The inset shows the spin−orbit split Re 4f peaks in detail. (b) XPS data of the Ru $3d_{5/2}$ for molecule **4** (orange) and **5** (green).

where ···−M−O−M−··· represents the adsorption sites on the oxide surface and R represents the particular dye minus the carboxyl group. The adsorption energy (E_{ads}) for dye **1** with two carboxyl anchors has been computed as

$$E^{ads} = E^{sub+mol} - E^{sub} - E^{mol} + E^{H_2}$$

where $E^{sub+mol}$ is the energy of the whole system, substrate [NiAl(110) + alumina] + adsorbed molecule on top, E^{sub} is the energy of the substrate alone, E^{mol} is the energy of the freestanding molecule, and E^{H_2} is the energy of the hydrogen molecule. This last term is doubled for dye **2**, as it has four H atoms in the two methylphosphonic acid anchors. Corresponding arguments apply to the methylphosphonic acid anchoring of molecule **2**. When the terminal H atoms are not removed from the molecules prior to the adsorption to the substrate, the adsorption energy is instead given by

$$E^{ads} = E^{sub+mol} - E^{sub} - E^{mol}$$

the corresponding reaction being of the sort

$$\cdots\text{−M−O−M−}\cdots + \text{R−CO−OH} \rightarrow \cdots\text{−M−O−M−O−C(OH)−R}$$

A different formulation is needed for dye **3**, because of the counterion:

$$E^{ads}_{dye3+OTf} = E^{sub+dye3+OTf} - E^{sub} - E^{dye3+OTf} + \frac{1}{2}E^{H_2}$$

for the H-dissociated case, where $E^{dye3+OTf}$ is the energy of dye **3** and the counterion together in the same supercell in vacuum, since both ions are not stable alone. For this reason, the adsorption energies for the individual ions cannot be separated easily. For the nondissociated case, the AE is

$$E^{ads}_{dye3+OTf} = E^{sub+dye3+OTf} - E^{sub} - E^{dye3+OTf}$$

RESULTS AND DISCUSSION

Self-assembled monolayers (SAMs) of the respective dyes are formed from solutions on clean ultrathin alumina films grown on a NiAl(110) crystal[26] in a custom-built chamber attached to our ultrahigh-vacuum system. The areal densities of the chemisorbed molecules are quantified by means of XPS data, and the coadsorption of the counterions for molecules **3** and **5** is also discussed. DFT calculations provide insight on the adsorption geometry and its effects on the electronic structure of the rhenium-based dye molecules. Hence, the three rhenium dyes are compared on the basis of UPS and DFT results. In order to more properly align the experimental UPS data and the calculated densities of states (DOS), we discuss the dynamical charge screening associated with the photoemission process in such systems.[45,46] This effect is of general relevance for comparing DFT results with experimental UPS data in organic and inorganic semiconductors.

Density of Molecules on the Surface. First, we characterize the dye monolayers using XPS to quantify the areal densities. Figure 2a shows the XPS data of the Al 2p, Ni 3p, and Re 4f core levels for the 2L-alumina substrate and the SAMs of the rhenium dyes. The metallic Al 2p and Ni 3p substrate peaks at 72 and 67 eV dominate the spectra. Interfacial Al^{2+} and Al^{3+} in the 2L-alumina film give rise to extra signals at higher binding energies.[47] Upon SAM deposition, a slight increase of the Al^{3+} component between 74 and 75 eV is observed, due to remaining impurities in the solvent and the tendency of 2L-alumina/NiAl(110) to further oxidation, as described in earlier work.[26] This rise is identical for all three molecules, and we quantify the total oxide thickness after molecule deposition to be 2.5 atomic layers.

The inset of Figure 2a compares the Re 4f peaks for dyes **1**, **2**, and **3**. Dyes **1** and **2** do not display significant differences in either binding energy or intensity. Both molecules have two covalent linkers located at the bipy group: dye **1** has two carboxyl groups, and dye **2** has two methylphosphonate groups. The additional atoms in the $DMPO_3$bipy do not alter the measured areal density (see Table 1). A slight shift to higher binding energies is, instead, observed for the Re 4f levels of dye **3**. On the other hand, for the dye **3** multilayer the shift is reversed (see Supporting Information, Figure 1a). This effect

Table 1. Areal Densities of the Molecules in the Monolayer, and the Average Molecule Diameters on the Surface[a]

molecule	density (nm^{-2})	diameter (nm)
1	1.32 ± 0.22	0.94 ± 0.16
2	1.34 ± 0.22	0.93 ± 0.15
3	1.07 ± 0.21	1.04 ± 0.20
4	0.69 ± 0.11	1.30 ± 0.21
5	0.64 ± 0.11	1.35 ± 0.24

[a]The numbers represent average values of densities or diameters obtained from different elemental core levels. Errors refer to 95% confidence interval.

DOI: 10.1021/acs.jpcc.9b05209
J. Phys. Chem. C 2019, 123, 22250−22260

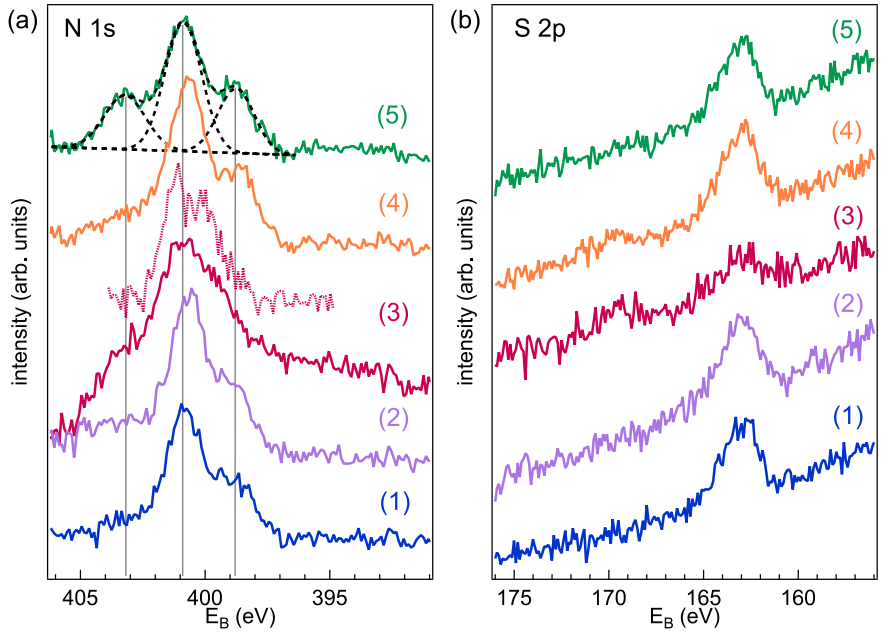

Figure 3. (a) Difference spectra of the N 1s peak − a Ni LMM Auger line from the substrate is present in the energy window of the N 1s peak when measured with a Mg Kα source. We obtain the difference spectra by subtracting a scaled substrate spectrum from the spectra obtained after molecule deposition. The dashed line is a reference measurement with Al Kα radiation for molecule **3**. A fit for molecule **5** (black) indicates the three occurring nitrogen species. Vertical lines mark the positions of the maxima. (b) XPS of the S 2p peak for the monolayer coverage of all molecules. Data for molecule **1** are reprinted from ref 26.

could be associated with the anchoring mode of the molecule to the surface or by a remaining positive net charge, if there is a lack of counterions on the surface. Further, we obtain a lower coverage for dye **3**, where the single carboxyl linker is part of the axial niacin group. The lower coverage suggests that the molecule requires significantly more space to be accommodated on the surface when the niacin linker replaces the thiocyanate.

Figure 2b displays the Ru $3d_{5/2}$ peaks of the ruthenium dyes **4** and **5**. The two dyes have almost the same structure, with **5** being the twice-deprotonated version of **4**, plus there are two TBA counterions. Therefore, even if the intensity is slightly lower for molecule **5**, the spectra appear rather similar.

Table 1 reports the calculated areal densities and deduced diameters of the five dyes, determined from the measured XPS intensities of the S 2p, N 1s, and Re 4f or Ru $3d_{5/2}$ peak (see Supporting Information, section S2). When comparing the densities of the molecular monolayers, we find that the rhenium dyes exhibit a significantly higher coverage than the ruthenium dyes. Monolayers of dye **4** were extensively studied on titania, showing multiconformational adsorption.[11,13] Ikeda et al. showed via scanning tunneling microscopy that intermolecular distances are typically in the order of 1.2−1.6 nm,[9] which is in good agreement with the average molecule diameter we obtain from the molecular density of molecule **4** (see Table 1). Surprisingly, for dyes **4** and **5** we obtain very similar densities, in spite of the TBA counterions, which are relatively large and, if coadsorbed, should occupy a significant amount of space. This finding is in line with an XPS study of the same dyes adsorbed from solution on nanostructured TiO_2,[7] where N719 (dye **5** showed 0.9 times the density of N3 (dye **4**).

Counterion Coadsorption. The coadsorption of the TBA counterions is manifest from the N 1s XPS data. Figure 3a shows the N 1s spectra of the five molecules. Molecule **1**, **2**, **4**, and **5** have nitrogen atoms in the bipy and the thiocyanate in a ratio of 2:1, which we identified at 400.9 and 398.8 eV, respectively.[26] Molecule **5** exhibits a third peak at 403.2 eV due to the coadsorption of TBA. The intensity ratio of 0.95:2.01:1.00 ($I_{TBA}/I_{bipy}/I_{NCS}$) between the three peaks confirms that the original stoichiometry is preserved upon adsorption. This result is in contrast to observations on nanostructured TiO_2[7,10] and TiO_2(001),[48] where XPS revealed a significant loss of TBA counterions. This can be rationalized by considering the higher acidity of the TiO_2 as compared to alumina[49] together with the protic solvent (EtOH) used the authors of the studies on TiO_2.[7,48] Together with the observed similar areal density as molecule **4**, our results suggest a saltlike bonding where molecule **5** binds directly to the surface and counterions form ionic bonds within the monolayer to preserve charge neutrality.

Molecule **3** contains nitrogen atoms in the bipy and the axial niacin ligand. The N 1s spectrum of the multilayer exhibits one distinct peak at approximately 400.9 eV due to these three nitrogen atoms (see Supporting Information, section S1, Figure 1d), which are chemically similar. For the monolayer, however, this peak broadens significantly (see Supporting Information, section S1, Figure 1d), as also confirmed by an independent measurement with a monochromatic Al Kα source (Figure 3a). The molecule binds via the carboxyl group on the axial niacin ligand, and we speculate that different adsorption geometries might stress the bond between the pyridine and the rhenium, leading to a distribution of different chemical environments for the nitrogen atoms.

Dyes **1**, **2**, **4**, and **5** contain thiocyanate, which we identify from the S 2p peak, clearly recognizable from the spectra in Figure 3b. The S $2p_{3/2}$ peak[50] has a binding energy of 162.8 eV. For dye **1**, **2**, and **5**, this is the only species observed; thus, we deduce that the binding of sulfur in the thiocyanate groups with oxygen atoms in the surface is unlikely for these cases.

DOI: 10.1021/acs.jpcc.9b05209
J. Phys. Chem. C 2019, 123, 22250−22260

Previous work on dyes **4** and **5** indicated that binding of thiocyanate to oxygen atoms in the surface leads to significant chemical shifts.[8,48] For dye **4**, we observe a second minor species with the S $2p_{3/2}$ at 169.7 eV, a binding energy typical for sulfur bonds in sulfate- or sulfone-like environments.[50] This indicates that some molecules have adsorption geometries where sulfur−oxygen interaction occurs. Interestingly, this interaction seems to be avoided by molecule **5**; hence, we speculate that the presence of the counterions changes the ensemble of adsorption geometries.

Dye **3** itself does not contain sulfur, but it is present in the OTf counterion ($CF_3SO_3^-$). We observe two S 2p species at 162.8 and 169.2 eV (these binding energies refer to the S $2p_{3/2}$ peak). We identify the smaller peak at 169.2 eV as the contribution from the intact OTf counterion, which dominates the S 2p spectrum of the multilayer (see Supporting Information, section S1, Figure 1b). The second feature appears to be the remnant of decomposed counterions, as a deficit of fluorine signal in the monolayer suggests (see Supporting Information, section S1, Figure 1c). When comparing the total amount of rhenium to the amount of adsorbed sulfur from both species, we find a ratio of 1.0:0.8. This ratio indicates a nearly stoichiometric coadsorption of the counterions in the monolayer. The decomposition of the OTf by release of fluorine might be activated at oxygen-deficient line defects present on the 2L-alumina surface, which can behave as native electron donors.[51]

In summary, the XPS data corroborate the structural integrity of all five dyes upon adsorption and furthermore show coadsorption of counterions in the cases of the two dyes carrying charges.

Structural Models of the Adsorbed Re Dyes. We used DFT calculations to find the most stable adsorption configurations for dyes **1**, **2**, and **3**. For dyes **4** and **5**, we refer to a range of studies from other groups.[11−13,52,53] To model the experimental substrate we employ a 2L-alumina formed by oxidation of NiAl(110). The unit cell dimension and atomic coordinates of the oxide are taken from Kresse et al.,[24] while the NiAl unit cell is taken from The Materials Project.[54] The NiAl crystal structure is cut along the (110) direction, maintaining the stoichiometry. A slight lateral strain is required in order to match the alumina lattice. This unit cell has then been doubled and cut accordingly to create a parallelogram-shaped supercell[24,55] with a total of 327 atoms (see Supporting Information, section S3), where the alumina is in contact with two layers of NiAl(110). These two bottom layers have been kept fixed in all geometry optimizations. The layer-resolved DOS of the aluminum oxide film on NiAl(110) (see Supporting Information, section S4) shows the hybridization taking place between the interfacial Al atoms and the NiAl substrate.[24]

For each molecule we considered several initial configurations in the search for the most stable geometry. For dye **1**, we explored the possibility of nondissociative and dissociative adsorption, i.e., by removing some of the terminal hydrogens from the anchoring groups, and considered different orientations of the dyes on the surface. In the case of dye **3**, we also took into account the coadsorption of the counterion in the vicinity of the dye as well as the charge state of the adsorbed species. Adsorption generally occurs via the formation of covalent bonds between the double-bonded oxygen of the carboxyl or the methylphosphonic acid and one under-coordinated Al atom at the surface, which is slightly displaced upward (see Figure 4).

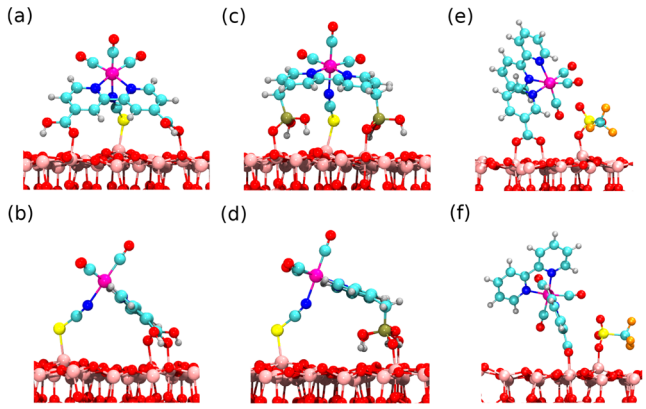

Figure 4. Two lateral views of the most stable adsorption configurations of the rhenium dyes on alumina: dye **1** in panels a and b, dye **2** in panels c and d, and dye **3** in panels e and f. Color code: Re (purple), Al (pink), O (red), S (yellow), N (blue), C (cyan), H (white), P (gold), F (orange).

Dyes **1** and **2** present similar features: The most stable structure exhibits two anchor−O−Al bonds, one per linker, and no dissociation of further hydrogen occurs. A third anchoring point is represented by the thiocyanate, forming a dye−S−Al bond and causing a significant distortion of the molecule. In particular, the less rigid $DMPO_3$bipy linkers of dye **2** allows the positioning of the bipy almost parallel to the surface plane. The corresponding adsorption energies are reported in Table 2. These are computed taking as reference the optimized pristine thin film and the dye equilibrated in vacuum.

Table 2. Adsorption Energies (AE) Computed for the Most Stable Configurations of the Three Intact Re Dyes When the Hydrogen Atoms of the Linkers Remain Bound to the Respective Acid (Left) or When They Are Removed (Right)[a]

molecule	AE with H's (eV)	AE without H's (eV)
1	−3.01	−2.87
2	−4.24	−3.71
3	−1.40	−3.64

[a]Note that in the case of dye **3** the AE contains the combined contribution of the coadsorbed dye and counterion.

To simulate a situation where additional anchor−O−Al bonds can be formed, we also estimated the activation energy required to transfer one H atom from one anchoring group of the adsorbed dye **1** to the surface. The reaction path has been obtained by applying a nudged elastic band procedure[56] where the final state consists of the adsorbed H-dissociated molecule and the two dissociated H atoms placed at nearby surface O atoms. The resulting energy barrier amounts to about 1.5 eV (see Supporting Information, section S5), and the final configuration is less stable than the initial one, where the dye is not yet dissociated, and also it is less stable than the case where the H atoms are assumed to leave the surface as a H_2 molecule. Therefore, we conclude that the nondissociative adsorption is the most probable for dye **1**. The same

DOI: 10.1021/acs.jpcc.9b05209
J. Phys. Chem. C 2019, 123, 22250−22260

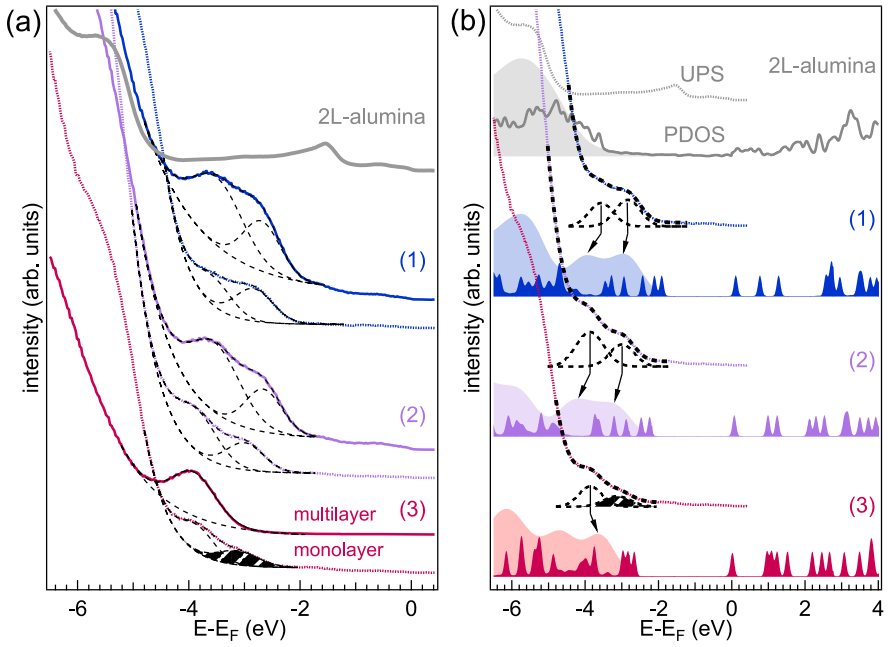

Figure 5. (a) UPS data of monolayers (dotted lines) and multilayers (solid lines) of the rhenium dyes **1** (blue), **2** (violet), **3** (red), and the 2L-alumina/NiAl(110) substrate (gray). Peaks in the band gap of 2L-alumina are fitted with Gaussian functions and exponential background (black dashed lines). The shaded area indicates the extra feature in the monolayer of dye **3**. Data for molecule **1** is reprinted from ref 26. (b) Comparison of the UPS data of the substrate and the dye monolayers (dashed lines) with the PDOS (dark-shaded areas: PDOS with σ = 50 meV Gaussian energy broadening). The light-shaded areas illustrate the broadening and shifting due to hole-screening on the PDOS (see text) and can be compared to the experimental spectra. Arrows assign observed peaks in the UPS data to features in the modified PDOS. For clarity, a multiplier of 10 is used for the PDOS of the unoccupied states in the alumina.

conclusion is also valid for dye **2**. Table 2 reports also the adsorption energies calculated for the dyes without H atoms at the linkers, where we consider the hydrogen molecule in the gas phase as the reference state for the dissociated hydrogen.

Dye **3** binds via the axial niacin ligand, and the most stable adsorption state corresponds to the formation of two anchor−O−Al bonds, i.e., it is dissociative. The OTf counterion ($CF_3SO_3^-$) binds to the surface through an oxygen atom, while the fluorine does not form any bond with the substrate. The adsorption energy computed considering the counterion coadsorption is −3.64 eV.

The reported data are related to the most stable structure with and without terminal hydrogens. Actually, for both situations, more geometries have been found that are stable, with adsorption energies that vary in a range of 2 eV, depending on the number of bonds to the surface and on the internal distortion of the molecule. Some of the alternative adsorption geometries are quite close in energy to the discussed lowest minima. This suggests that multiconformational adsorption similar to what was described by Kley et al.[13] for dye **4** on TiO_2 is likely also for the rhenium dyes described here.

In summary, we find that the expected anchoring modes via the carboxyl groups or the methylphosphonic acid groups present the most stable bonding geometries, with the additional unexpected dye−S−Al bonds further stabilizing the bonding of dyes **1** and **2**. We therefore use these configurations for discussing the energy alignment of the frontier orbitals with the alumina band edges.

Electronic Structure. To characterize the electronic structure of the metal/insulator/dye interface we analyze UPS and DFT results. Figure 5a compares the UPS data of the 2L-alumina substrate and the three rhenium dyes in the mono- and multilayer coverage. Multilayer refers to 2.4 layers for dye **1**,[26] 1.5 layers for dye **2**, and 7.8 layers for dye **3**. Exposure to the solution was similar in all cases, different multilayer coverages might originate from different solubilities and kinetic factors. The band structure of 2L-alumina was previously discussed in the literature.[23,25] The hybridization of interfacial atoms in 2L-alumina with the substrate causes a nonvanishing density of states in the band gap (see Supporting Information, section S4, for the layer-resolved DOS). The UPS spectral features in the energy interval of −4 eV up to the Fermi energy are attributed to the metallic NiAl(110) substrate.[23,25] The edge of the valence band of 2L-alumina is detected below −4 eV. The spectra of dyes **1** and **2** show two peaks in the band gap of 2L-alumina, appearing both in the mono- and multilayer coverage. The UPS spectrum of the multilayer of dye **3** shows one single peak in the same energy range, whereas its monolayer presents one additional peak at −3.1(6) eV (shaded area). This additional peak could be caused by the deprotonated character of dye **3** in the adsorbed state, as suggested by our structural optimization using DFT, or by decomposed OTf. The peak parameters are summarized in Table 3. Experimental UPS data for the ruthenium-based dyes and the corresponding interpretation are available in the Supporting Information (section S6).

Figure 5b compares the UPS data obtained for the dye monolayers with the projected density of states (PDOS) resulting from the DFT-optimized adsorbate structures shown in Figure 4. The electronic structure analysis is performed at the HSE06[44] level of theory, on the geometries obtained at the PBE level of theory. We apply a Gaussian convolution with σ = 50 meV to the PDOS histogram (dark-shaded area for

DOI: 10.1021/acs.jpcc.9b05209
J. Phys. Chem. C 2019, 123, 22250−22260

Table 3. Peak Maxima and Onsets of the Peaks Found by UPS for Mono- and Multilayers[a]

molecule		peak 1 (eV)	peak 2 (eV)
1	monolayer	−2.8(5) [−2.1(5)]	−3.5(6) [−2.9(3)]
	multilayer	−2.7(3) [−2.0(3)]	−3.5(2) [−2.7(1)]
2	monolayer	−2.9(7) [−2.3(2)]	−3.8(7) [−3.0(6)]
	multilayer	−2.6(4) [−1.9(9)]	−3.5(4) [−2.5(5)]
3	monolayer	−3.1(6) [−2.3(9)]	−3.8(6) [−3.2(6)]
	multilayer		−3.9(1) [−3.1(3)]
4	monolayer	−2.1(4) [−1.4(4)]	−3.4(4) [−2.7(9)]
5	monolayer	−2.2(4) [−1.4(4)]	−3.5(6) [−2.7(8)]

[a]The onsets are denoted in squared brackets. They are determined by linear extrapolation of the rising edge of the peak and its crossing with the background at higher energy (see Supporting Information, section S8).

molecules and gray line for 2L-alumina in Figure 5b), which reflects the experimental energy resolution. The observed features in the UPS data are significantly broader and shifted to higher binding energies. Previously, Krause et al. deduced that dynamic hole delocalization in response to the photoexcitation plays a major role for the interpretation of UPS data of organic[45] and inorganic semiconductors.[46] They concluded that the peak onsets in UPS data mark the positions of electronic levels relevant for the transport gap. We adopt the same reasoning for our heterogeneous systems and broaden and shift the PDOS correspondingly (see Supporting Information, section S8) in order to make a comparison of experimental and theoretical data. We apply the same broadening and shift to the PDOS of all systems (light-shaded area in Figure 5b). The result compares well to the experimental UPS data: for dyes **1** and **2** we find the characteristic two peaks in the band gap of 2L-alumina, and for dye **3** one peak. Since the level alignment was found to be rather sensitive to the particular bonding geometry adopted for the molecules, this agreement supports the validity of the optimized structures shown in Figure 4.

Figure 6a shows the energy alignment of the HOMOs and LUMOs (DFT values only) of the three rhenium dyes on 2L-alumina and compares the experimental values with the ones derived from the DFT. For all dyes, the HOMO as well as the LUMO lie in the band gap of the substrate. We use the values of the valence band maximum, the conduction band minimum, and the work function of the 2L-alumina/NiAl(110) substrate from the literature.[25,57] The values of the peak onsets derived from the UPS data (Table 3) are in good agreement with the HOMO energy levels from the DFT with deviations of less than 300 meV. The experimental and computational values indicate the same trend for the alignment of the HOMOs, with **1** being the closest to the Fermi level and **3** the farthest away. The DFT locates the LUMOs of all three dyes closely above the Fermi level.

Figure 6b displays the density distribution of the HOMOs and LUMOs of the three adsorbed rhenium dyes. For all dyes, the HOMO is mostly located on the rhenium center. Dyes **1** and **2** are peculiar, as their HOMOs reside prevalently on the sulfur in the thiocyanate in the gas phase (Supporting Information, section S9). After adsorption onto the substrate, it is instead localized mainly on the Re atom. This change could be caused by a charge transfer taking place with the formation of the S−Al bond. Dye **3** has a +1 charge that is delocalized on the pyridine rings, while the HOMO has Re and C contributions, since the sulfur atom is part of the counterion. All LUMOs, on the other hand, are mainly located on the carbon rings of the bipy. A more detailed analysis of the

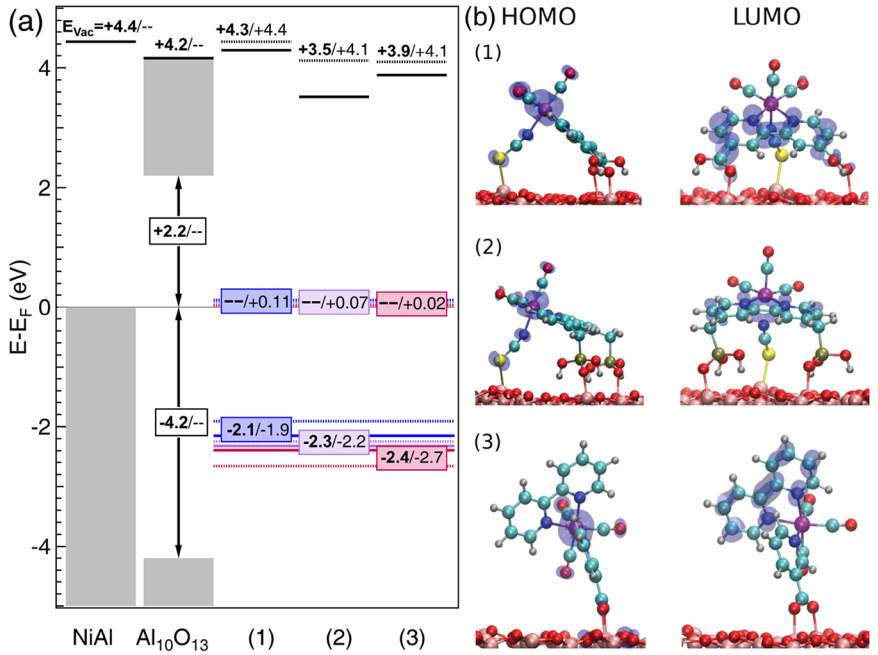

Figure 6. (a) Energy alignment of the HOMO and LUMO of the three rhenium dyes in the dye/2L-alumina/NiAl(110) heterojunction. The energy levels of the HOMOs, the LUMOs, and the vacuum levels are represented as solid lines, and the values derived from the DFT as dashed lines. Experimental values are on the left in bold, and values derived from the DFT are written on the right. (b) Orbitals corresponding to the HOMOs (left side) and LUMOs (right side) of the three rhenium dyes, at the PBE level of theory, on 2L-alumina. The isosurfaces are taken, in vacuum, at 0.02 au for all HOMOs, while the LUMO isosurfaces are taken at 0.002, 0.01, and 0.005 au for dyes **1**, **2**, and **3**, respectively.

DOI: 10.1021/acs.jpcc.9b05209
J. Phys. Chem. C 2019, 123, 22250−22260

density of states of the different dyes (see Supporting Information, sections S7 and S8) assesses the contributions of the different atomic species to the molecular orbitals.

The close proximity of the LUMO to the Fermi level for all three adsorbed Re dyes is favorable for resonant tunneling of excited electrons from the dye through the alumina film to the underlying substrate, supported also by the strong covalent bonding to the alumina layer. For a high tunneling probability, the spatial overlap of the LUMO with the substrate wave functions should be maximized, i.e., the LUMO should be localized close to the anchoring groups. The DFT results shown in Figure 6b suggest that electron injection via tunneling should be most effective with dye **1** and least effective with dye **3**.

CONCLUSIONS

We have characterized the bonding geometry and the electronic structure of five systematically altered organometallic dyes on alumina, trying to address the physical parameters of the systems that are relevant for tunneling-based electron transfer from photoexcited dyes to the underlying substrate. XPS data from dye monolayers give confidence that the molecules are deposited intact and bind covalently to the alumina surface. Likewise, the comparison of the occupied molecular orbital energies obtained from DFT calculations with the values measured with UPS supports the validity of the proposed anchoring configurations. The binding energy of the HOMO of dye **1** is the lowest among the rhenium dyes, followed by **2**, and **3** having the highest binding energy. When comparing UPS measurements with the calculated PDOS, the observed peaks are significantly broadened and shifted to higher binding energies in the photoemission data. We attribute this to dynamic charge screening during the photoemission process.[45,46] This effect should be of general relevance for investigations of molecules on oxide surfaces. The consideration of charge screening is crucial when comparing UPS or angle-resolved photoemission spectroscopy data with the calculated electronic states or band structure and deducing the energy level alignment in heterojunctions.

Dyes **1** and **2** show a similar behavior regarding coverage, electronic structure, and binding to the surface, including the extra anchoring via the thiocyanate group. The latter suggests that thiocyanate groups can play a significant role for the adsorption on oxides, in particular if the oxide surface has exposed metal ions. The main difference between the two dyes is that, while the methylphosphonic acid groups bind more strongly to the alumina than the carboxyl anchors, they distance the LUMO further away from the surface. Electron injection via tunneling should thus be less efficient with dye **2**.

The anchoring via the axial niacin ligand distinguishes dye **3** from dyes **1** and **2**. It places the LUMO even farther away from the surface, farther away in fact than the HOMO. Upon photoexcitation, this configuration might lead to a reversal of the charge transfer, i.e., to electron transfer from the substrate into the dye. In contrast to dyes **1** and **2**, the binding to the surface is strongly stabilized by dissociating the hydrogen atom from the anchoring group.

Dyes **3** and **5** carry charges, and we could show that the respective OTf and TBA counterions adsorb both nearly stoichiometrically. In spite of the presence of these extra charges within the adsorbed molecular monolayer, the alignment of the occupied molecular orbitals relative to the alumina valence band edge is only weakly affected in both cases, but in both cases the effect leads to a slightly higher binding energy (see Supporting Information section S6 for the UPS data of dye **5**). The areal densities of the molecules **4** and **5** are nearly identical, which indicates that the coadsorbed TBA counterions do not require a significant additional amount of space on the surface.

Given this set of dyes with different anchoring modes, it will be interesting to study and compare the dynamics of the photoinduced charge transfer processes, either with the core–hole clock method[18] or with ultrafast photoelectron spectroscopy in pump–probe mode,[58] in order to confirm the link between the physical parameters determined in our study and the actual dynamics of tunneling through the alumina layer.

ASSOCIATED CONTENT

Supporting Information

The Supporting Information is available free of charge on the ACS Publications website at DOI: 10.1021/acs.jpcc.9b05209.

XPS data of dye **3** in the mono- and multilayer, areal density of different atomic species and calculation of molecular density, aluminum oxide film on NiAl(110), DOS of Al_2O_3, hydrogen removal barrier, UPS measurements of ruthenium-based dyes, PDOS of the rhenium dyes on 2L-alumina, influence of charge-screening in UPS, HOMOs and LUMOs in vacuum, and synthesis of rhenium complexes (PDF)

AUTHOR INFORMATION

Corresponding Author

*E-mail: osterwal@physik.uzh.ch.

ORCID

Wolf-Dietrich Zabka: 0000-0002-4949-6495
Zbynek Novotny: 0000-0002-3575-7535
Marcella Iannuzzi: 0000-0001-9717-2527
Benjamin Probst: 0000-0001-8850-9685
Roger Alberto: 0000-0001-5978-3394
Jürg Osterwalder: 0000-0001-9517-641X

Notes

The authors declare no competing financial interest.

ACKNOWLEDGMENTS

The authors thank Jürg Hutter, Thomas Moehl, and David Tilley for helpful discussions. This project has been financed under the University Research Priority Program LightChEC of the University of Zurich and a Sinergia project of the Swiss National Science Foundation (CRSII2_160801 /1). We thank the Swiss National Supercomputer Centre (CSCS) under projects ID s657 and uzh1 for computational resources.

REFERENCES

(1) Grätzel, M. Photoelectrochemical Cells. *Nature* **2001**, *414*, 338.
(2) Hagfeldt, A.; Boschloo, G.; Sun, L.; Kloo, L.; Pettersson, H. Dye-Sensitized Solar Cells. *Chem. Rev.* **2010**, *110*, 6595–6663.
(3) Swierk, J. R.; Mallouk, T. E. Design and Development of Photoanodes for Water-Splitting Dye-Sensitized Photoelectrochemical Cells. *Chem. Soc. Rev.* **2013**, *42*, 2357–2387.
(4) Yu, Z.; Li, F.; Sun, L. Recent Advances in Dye-Sensitized Photoelectrochemical Cells for Solar Hydrogen Production Based on Molecular Components. *Energy Environ. Sci.* **2015**, *8*, 760–775.
(5) Xu, P.; McCool, N. S.; Mallouk, T. E. Water Splitting Dye-Sensitized Solar Cells. *Nano Today* **2017**, *14*, 42–58.

DOI: 10.1021/acs.jpcc.9b05209
J. Phys. Chem. C 2019, 123, 22250–22260

(6) Zhang, L.; Cole, J. M. Anchoring Groups for Dye-Sensitized Solar Cells. *ACS Appl. Mater. Interfaces* **2015**, *7*, 3427−3455.
(7) Johansson, E. M. J.; Hedlund, M.; Siegbahn, H.; Rensmo, H. Electronic and Molecular Surface Structure of $Ru(tcterpy)(NCS)_3$ and $Ru(dcbpy)_2(NCS)_2$ Adsorbed from Solution onto Nanostructured TiO_2: A Photoelectron Spectroscopy Study. *J. Phys. Chem. B* **2005**, *109*, 22256−22263.
(8) Mayor, L. C.; Ben Taylor, J. B.; Magnano, G.; Rienzo, A.; Satterley, C. J.; O'Shea, J. N.; Schnadt, J. Photoemission, Resonant Photoemission, and X-Ray Absorption of a Ru(II) Complex Adsorbed on Rutile $TiO_2(110)$ Prepared by In Situ Electrospray Deposition. *J. Chem. Phys.* **2008**, *129*, 114701.
(9) Ikeda, M.; Koide, N.; Han, L.; Pang, C. L.; Sasahara, A.; Onishi, H. Lateral Distribution of N3 Dye Molecules on $TiO_2(110)$ Surface. *J. Photochem. Photobiol., A* **2009**, *202*, 185−190.
(10) Lee, K. E.; Gomez, M. A.; Regier, T.; Hu, Y.; Demopoulos, G. P. Further Understanding of the Electronic Interactions between N719 Sensitizer and Anatase TiO_2 Films: A Combined X-ray Absorption and X-ray Photoelectron Spectroscopic Study. *J. Phys. Chem. C* **2011**, *115*, 5692−5707.
(11) Martsinovich, N.; Ambrosio, F.; Troisi, A. Adsorption and Electron Injection of the N3Metal−Organic Dye on the TiO_2 Rutile (110) Surface. *Phys. Chem. Chem. Phys.* **2012**, *14*, 16668−16676.
(12) Weston, M.; Reade, T. J.; Handrup, K.; Champness, N. R.; O'Shea, J. N. Adsorption of Dipyrrin-Based Dye Complexes on a Rutile $TiO_2(110)$ Surface. *J. Phys. Chem. C* **2012**, *116*, 18184−18192.
(13) Kley, C. S.; Dette, C.; Rinke, G.; Patrick, C. E.; Čechal, J.; Jung, S. J.; Baur, M.; Dürr, M.; Rauschenbach, S.; Giustino, F.; et al. Atomic-Scale Observation of Multiconformational Binding and Energy Level Alignment of Ruthenium-Based Photosensitizers on TiO_2 Anatase. *Nano Lett.* **2014**, *14*, 563−569.
(14) Le Formal, F.; Tétreault, N.; Cornuz, M.; Moehl, T.; Grätzel, M.; Sivula, K. Passivating Surface States on Water Splitting Hematite Photoanodes with Alumina Overlayers. *Chem. Sci.* **2011**, *2*, 737−743.
(15) Natu, G.; Huang, Z.; Ji, Z.; Wu, Y. The Effect of an Atomically Deposited Layer of Alumina on NiO in P-type Dye-Sensitized Solar Cells. *Langmuir* **2012**, *28*, 950−956.
(16) Ji, Z.; He, M.; Huang, Z.; Ozkan, U.; Wu, Y. Photostable p-Type Dye-Sensitized Photoelectrochemical Cells for Water Reduction. *J. Am. Chem. Soc.* **2013**, *135*, 11696−11699.
(17) Prasittichai, C.; Avila, J. R.; Farha, O. K.; Hupp, J. T. Systematic Modulation of Quantum (Electron) Tunneling Behavior by Atomic Layer Deposition on Nanoparticulate SnO_2 and TiO_2 Photoanodes. *J. Am. Chem. Soc.* **2013**, *135*, 16328−16331.
(18) Gibson, A. J.; Temperton, R. H.; Handrup, K.; Weston, M.; Mayor, L. C.; O'Shea, J. N. Charge Transfer from an Adsorbed Ruthenium-Based Photosensitizer through an Ultra-Thin Aluminium Oxide Layer and into a Metallic Substrate. *J. Chem. Phys.* **2014**, *140*, 234708.
(19) Katz, M. J.; DeVries Vermeer, M. J.; Farha, O. K.; Pellin, M. J.; Hupp, J. T. Dynamics of Back Electron Transfer in Dye-Sensitized Solar Cells Featuring 4-tert-Butyl-Pyridine and Atomic-Layer-Deposited Alumina as Surface Modifiers. *J. Phys. Chem. B* **2015**, *119*, 7162−7169.
(20) Mäkinen, V.; Honkala, K.; Häkkinen, H. Atomic Layer Deposition of Aluminum Oxide on TiO_2 and Its Impact on N3 Dye Adsorption from First Principles. *J. Phys. Chem. C* **2011**, *115*, 9250−9259.
(21) Antila, L. J.; Heikkilä, M. J.; Mäkinen, V.; Humalamäki, N.; Laitinen, M.; Linko, V.; Jalkanen, P.; Toppari, J.; Aumanen, V.; Kemell, M.; et al. ALD Grown Aluminum Oxide Submonolayers in Dye-Sensitized Solar Cells: The Effect on Interfacial Electron Transfer and Performance. *J. Phys. Chem. C* **2011**, *115*, 16720−16729.
(22) Terranova, U.; Bowler, D. R. Coating TiO_2 Anatase by Amorphous Al_2O_3: Effects on Dyes Anchoring Through Carboxyl Groups. *J. Phys. Chem. C* **2012**, *116*, 4408−4415.
(23) Jaeger, R. M.; Kuhlenbeck, H.; Freund, H.-J.; Wuttig, M.; Hoffmann, W.; Franchy, R.; Ibach, H. Formation of a Well-Ordered Aluminium Oxide Overlayer by Oxidation of NiAl(110). *Surf. Sci.* **1991**, *259*, 235−252.
(24) Kresse, G.; Schmid, M.; Napetschnig, E.; Shishkin, M.; Köhler, L.; Varga, P. Structure of the Ultrathin Aluminum Oxide Film on NiAl(110). *Science* **2005**, *308*, 1440−1442.
(25) Zabka, W.-D.; Leuenberger, D.; Mette, G.; Osterwalder, J. From Two- to Three-Dimensional Alumina: Interface Templated Films and Formation of γ-$Al_2O_3(111)$ Nuclei. *Phys. Rev. B: Condens. Matter Mater. Phys.* **2017**, *96*, 155420.
(26) Zabka, W.-D.; Mosberger, M.; Novotny, Z.; Leuenberger, D.; Mette, G.; Kälin, T.; Probst, B.; Osterwalder, J. Functionalization and Passivation of Ultrathin Alumina Films of Defined Sub-Nanometer Thickness with Self-Assembled Monolayers. *J. Phys.: Condens. Matter* **2018**, *30*, 424002.
(27) Hagfeldt, A.; Grätzel, M. Molecular Photovoltaics. *Acc. Chem. Res.* **2000**, *33*, 269−277.
(28) Gillaizeau-Gauthier, I.; Odobel, F.; Alebbi, M.; Argazzi, R.; Costa, E.; Bignozzi, C. A.; Qu, P.; Meyer, G. J. Phosphonate-Based Bipyridine Dyes for Stable Photovoltaic Devices. *Inorg. Chem.* **2001**, *40*, 6073−6079.
(29) Stufkens, D. J.; Vlček, A. Ligand-Dependent Excited State Behaviour of Re(I) and Ru(II) Carbonyl-Diimine Complexes. *Coord. Chem. Rev.* **1998**, *177*, 127−179.
(30) Costa, I.; Montalti, M.; Pallavicini, P.; Perotti, A.; Prodi, L.; Zaccheroni, N. Absorption and Luminescence as a Function of pH for Carboxylic Acid-Functionalized Re(I) Tricarbonyls. *J. Organomet. Chem.* **2000**, *593*−*594*, 267−273.
(31) Dattelbaum, D. M.; Omberg, K. M.; Hay, P. J.; Gebhart, N. L.; Martin, R. L.; Schoonover, J. R.; Meyer, T. J. Defining Electronic Excited States Using Time-Resolved Infrared Spectroscopy and Density Functional Theory Calculations. *J. Phys. Chem. A* **2004**, *108*, 3527−3536.
(32) Greber, T.; Raetzo, O.; Kreutz, T. J.; Schwaller, P.; Deichmann, W.; Wetli, E.; Osterwalder, J. A Photoelectron Spectrometer for k-Space Mapping above the Fermi Level. *Rev. Sci. Instrum.* **1997**, *68*, 4549−4554.
(33) Seah, M. P. Summary of ISO/TC 201 Standard: VII ISO 15472:2001 − Surface Chemical Analysis − X-Ray Photoelectron Spectrometers − Calibration of Energy Scales. *Surf. Interface Anal.* **2001**, *31*, 721−723.
(34) Scofield, J. Hartree-Slater Subshell Photoionization Cross-Sections at 1254 and 1487 eV. *J. Electron Spectrosc. Relat. Phenom.* **1976**, *8*, 129−137.
(35) Tanuma, S.; Powell, C. J.; Penn, D. R. Calculations of Electron Inelastic Mean Free Paths. V. Data for 14 Organic Compounds over the 50−2000 eV Range. *Surf. Interface Anal.* **1994**, *21*, 165−176.
(36) Hutter, J.; Iannuzzi, M.; Schiffmann, F.; VandeVondele, J. CP2K: Atomistic Simulations of Condensed Matter Systems. *WIREs Comput. Mol. Sci.* **2014**, *4*, 15−25.
(37) Perdew, J. P.; Burke, K.; Ernzerhof, M. Generalized Gradient Approximation Made Simple. *Phys. Rev. Lett.* **1996**, *77*, 3865−3868.
(38) Goedecker, S.; Teter, M.; Hutter, J. Separable Dual-Space Gaussian Pseudopotentials. *Phys. Rev. B: Condens. Matter Mater. Phys.* **1996**, *54*, 1703−1710.
(39) VandeVondele, J.; Hutter, J. Gaussian Basis Sets for Accurate Calculations on Molecular Systems in Gas and Condensed Phases. *J. Chem. Phys.* **2007**, *127*, 114105.
(40) VandeVondele, J.; Krack, M.; Mohamed, F.; Parrinello, M.; Chassaing, T.; Hutter, J. Quickstep: Fast and Accurate Density Functional Calculations Using a Mixed Gaussian and Plane Waves Approach. *Comput. Phys. Commun.* **2005**, *167*, 103−128.
(41) Grimme, S.; Antony, J.; Ehrlich, S.; Krieg, H. A Consistent and Accurate Ab Initio Parametrization of Density Functional Dispersion Correction (DFT-D) for the 94 Elements H-Pu. *J. Chem. Phys.* **2010**, *132*, 154104.
(42) Perdew, J. P.; Ernzerhof, M.; Burke, K. Rationale for Mixing Exact Exchange with Density Functional Approximations. *J. Chem. Phys.* **1996**, *105*, 9982−9985.

DOI: 10.1021/acs.jpcc.9b05209
J. Phys. Chem. C 2019, 123, 22250−22260

(43) Adamo, C.; Barone, V. Toward Reliable Density Functional Methods without Adjustable Parameters: The PBE0Model. *J. Chem. Phys.* **1999**, *110*, 6158−6170.
(44) Heyd, J.; Scuseria, G. E.; Ernzerhof, M. Hybrid Functionals Based on a Screened Coulomb Potential. *J. Chem. Phys.* **2003**, *118*, 8207−8215.
(45) Krause, S.; Casu, M.; Schöll, A.; Umbach, E. Determination of Transport Levels of Organic Semiconductors by UPS and IPS. *New J. Phys.* **2008**, *10*, 085001.
(46) Krause, S.; Schöll, A.; Umbach, E. Determination of Transport Levels of Inorganic Semiconductors by Ultraviolet and Inverse Photoemission. *Phys. Rev. B: Condens. Matter Mater. Phys.* **2015**, *91*, 195101.
(47) Martin, N. M.; Knudsen, J.; Blomberg, S.; Gustafson, J.; Andersen, J. N.; Lundgren, E.; Ingelsten, H. H.; Carlsson, P.-A.; Skoglundh, M.; Stierle, A.; et al. High-Resolution Core-Level Spectroscopy Study of the Ultrathin Aluminum Oxide Film on NiAl(110). *Phys. Rev. B: Condens. Matter Mater. Phys.* **2011**, *83*, 125417.
(48) Zuleta, M.; Yu, S.; Ahmadi, S.; Boschloo, G.; Göthelid, M.; Hagfeldt, A. Monitoring N719 Dye Configurations on (1 × n)-Reconstructed Anatase (100) by Means of STM: Reversible Configurational Changes upon Illumination. *Langmuir* **2010**, *26*, 13236−13244.
(49) Del Arco, M.; Holgado, M. J.; Martin, C.; Rives, V. Reactivity of Vanadia with Silica, Alumina, and Titania Surfaces. *Langmuir* **1990**, *6*, 801−806.
(50) Chastain, J.; King, R. C.; Moulder, J. *Handbook of X-Ray Photoelectron Spectroscopy: A Reference Book of Standard Spectra for Identification and Interpretation of XPS Data*; Physical Electronics Division, Perkin-Elmer Corporation: Eden Prairie, MN, 1992.
(51) Schmid, M.; Shishkin, M.; Kresse, G.; Napetschnig, E.; Varga, P.; Kulawik, M.; Nilius, N.; Rust, H.-P.; Freund, H.-J. Oxygen-Deficient Line Defects in an Ultrathin Aluminum Oxide Film. *Phys. Rev. Lett.* **2006**, *97*, 046101.
(52) De Angelis, F.; Fantacci, S.; Selloni, A. Alignment of the Dye's Molecular Levels with the TiO_2 Band Edges in Dye-Sensitized Solar Cells: a DFT−TDDFT Study. *Nanotechnology* **2008**, *19*, 424002.
(53) De Angelis, F.; Fantacci, S.; Mosconi, E.; Nazeeruddin, M. K.; Grätzel, M. Absorption Spectra and Excited State Energy Levels of the N719 Dye on TiO2 in Dye-Sensitized Solar Cell Models. *J. Phys. Chem. C* **2011**, *115*, 8825−8831.
(54) Jain, A.; Ong, S. P.; Hautier, G.; Chen, W.; Richards, W. D.; Dacek, S.; Cholia, S.; Gunter, D.; Skinner, D.; Ceder, G.; et al. The Materials Project: A Materials Genome Approach to Accelerating Materials Innovation. *APL Mater.* **2013**, *1*, 011002.
(55) Libuda, J.; Winkelmann, F.; Bäumer, M.; Freund, H.-J.; Bertrams, T.; Neddermeyer, H.; Müller, K. Structure and Defects of an Ordered Alumina Film on NiAl(110). *Surf. Sci.* **1994**, *318*, 61−73.
(56) Henkelman, G.; Uberuaga, B. P.; Jónsson, H. A Climbing Image Nudged Elastic Band Method for Finding Saddle Points and Minimum Energy Paths. *J. Chem. Phys.* **2000**, *113*, 9901−9904.
(57) Andersson, S.; Brühwiler, P. A.; Sandell, A.; Frank, M.; Libuda, J.; Giertz, A.; Brena, B.; Maxwell, A. J.; Bäumer, M.; Freund, H.-J.; et al. Metal-Oxide Interaction for Metal Clusters on a Metal-Supported Thin Alumina Film. *Surf. Sci.* **1999**, *442*, L964−L970.
(58) Borgwardt, M.; Wilke, M.; Kampen, T.; Mähl, S.; Xiao, M.; Spiccia, L.; Lange, K. M.; Kiyan, I. Y.; Aziz, E. F. Charge Transfer Dynamics at Dye-Sensitized ZnO and TiO2 Interfaces Studied by Ultrafast XUV Photoelectron Spectroscopy. *Sci. Rep.* **2016**, *6*, 24422.

DOI: 10.1021/acs.jpcc.9b05209
J. Phys. Chem. C 2019, 123, 22250−22260